of ~2 km for the Calico, Rodman, and Pinto Mountain faults, variations in the radar LOS displacements across the southern part of the Landers rupture are indicative of a rather narrow (several hundred meter wide) deformation zone (Fig. 1), apparently in agreement with the seismic studies. These observations suggest that the mechanical properties of seismogenic fault zones (the fault zone width, and the rigidity contrast with the surrounding rocks) may vary considerably, perhaps manifesting a cumulative damage from past earthquakes, and time-dependent healing in the interseismic period. If so, probing of the mechanical structure of seismogenic faults may help to identify various stages of the earthquake cycle for individual faults.

References and Notes

1. R. Sharp, M. Rymer, J. Lienkaemper, *Bull. Seismol. Soc. Am.* **76**, 949 (1986).
2. C. M. Poley, A. G. Lindh, W. H. Bakun, S. S. Schulz, *Nature* **327**, 134 (1987).
3. R. Harris, R. Simpson, P. Reasenberg, *Nature* **375**, 221 (1995).
4. E. Price, D. T. Sandwell, *J. Geophys. Res.* **103**, 27001 (1998).
5. T. Wright, E. Fielding, B. Parsons, *Geophys. Res. Lett.* **28**, 1079 (2001).
6. D. Sandwell, L. Sichoix, D. Agnew, Y. Bock, J.-B. Minster, *Geophys. Res. Lett.* **27**, 3101 (2000).
7. Y. Fialko, M. Simons, D. Agnew, *Geophys. Res. Lett.* **28**, 3063 (2001).
8. Previous inferences about the retrograde fault motion due to nearby earthquakes are uncertain because the interferometric data from only one look direction do not allow one to distinguish between the horizontal and vertical components of deformation.
9. If the retrograde fault displacement is due to frictional slip, the latter is more appropriately referred to as induced rather than triggered, because the causative stress change may not be small compared with the pre-existing stress.
10. Perpendicular baseline is a distance between the master and repeat satellite orbits in direction orthogonal to the radar line of sight. Small perpendicular baselines diminish sensitivity of the interferometric data to topography and reduce radar lay-overs in areas of steep topography.
11. T. G. Farr, M. Kobrick, *Eos* **81**, 583 (2000).
12. M. Simons, Y. Fialko, L. Rivera, *Bull. Seismol. Soc. Am.* **92**, 1390 (2002).
13. The nominal errors in the SRTM data are of the order of a few meters.
14. We normalize LOS displacements d_{los} by the cosine of the radar incidence angle to account for small but non-negligible variations in the incidence angle across the radar image.
15. P. Rosen *et al.* , *Proc. IEEE* **88**, 333 (2000).
16. For the orbital parameters of the ERS satellites, the along-fault displacement $U_{\parallel} \approx -1.21\Delta_{los}/\cos(\theta - 1.56)$, where θ is the fault strike in radians, provided that the fault-perpendicular displacement, $U_{\perp}$, is zero. A positive $U_{\parallel}$ displacement is left-lateral if θ is taken to be positive counterclockwise from North. For the Calico and Rodman faults striking ~35°NW, $U_{\parallel} \approx -2.1\Delta_{los}$. For the same fault geometry and assuming $U_{\parallel} = 0$, $U_{\perp} \approx -1.5\Delta_{los}$.
17. A. M. Rubin, *J. Geophys. Res.* **97**, 1839 (1992).
18. Y. A. Fialko, A. M. Rubin, *J. Geophys. Res.* **104**, 20,007 (1999).
19. The co-seismic stress changes shown in Fig. 3 are upper bounds because the shear modulus of the uppermost crust is likely less than the assumed value of 33 GPa. The lithostatic stress σ_l equals the weight of the overburden, $\sigma_l = \rho g z$, where ρ is the rock density, g is the gravitational acceleration, and z is depth. For $z = 1$ to 3 km, σ_l is of the order of tens of megapascals.
20. C. H. Scholz, *The Mechanics of Earthquakes and Faulting* (Cambidge Univ. Press, New York, 1990).
21. J. Byerlee, *Pure Appl. Geophys.* **116**, 615 (1978).
22. Y. Li, J. Vidale, K. Aki, C. Marone, W. Lee, *Science* **265**, 367 (1994).
23. Y. Li, W. Ellsworth, C. Thurber, P. Malin, K. Aki, *Bull. Seismol. Soc. Am.* **87**, 210 (1997).
24. Y. Ben-Zion, *J. Geophys. Res.* **103**, 12567 (1998).
25. Y. Li, J. Vidale, K. Aki, F. Xu, T. Burdette, *Science* **279**, 217 (1998).
26. R. Nikolaidis *et al.* , *J. Geophys. Res.* **106**, 21897 (2001).

27. We thank J. Vidale, P. Segall, and anonymous reviewers for their thoughtful comments. This work was supported by the Southern California Earthquake Center and NSF. Original InSAR data are copyright of the European Space Agency, distributed by Eurimage, Italy, and acquired via the WInSAR Consortium. The ERS SAR imagery was processed using the Caltech/JPL software package ROI_PAC.

Supporting Online Material

www.sciencemag.org/cgi/content/full/297/5588/1858/DC1

Figs. S1 and S2

4 June 2002; accepted 12 August 2002

Relative Timing of Deglacial Climate Events in Antarctica and Greenland

Vin Morgan,[1]* Marc Delmotte,[2,3]*† Tas van Ommen,[1]‡ Jean Jouzel,[3] Jérôme Chappellaz,[2] Suenor Woon,[1] Valérie Masson-Delmotte,[3] Dominique Raynaud[2]

The last deglaciation was marked by large, hemispheric, millennial-scale climate variations: the Bølling-Allerød and Younger Dryas periods in the north, and the Antarctic Cold Reversal in the south. A chronology from the high-accumulation Law Dome East Antarctic ice core constrains the relative timing of these two events and provides strong evidence that the cooling at the start of the Antarctic Cold Reversal did not follow the abrupt warming during the northern Bølling transition around 14,500 years ago. This result suggests that southern changes are not a direct response to abrupt changes in North Atlantic thermohaline circulation, as is assumed in the conventional picture of a hemispheric temperature seesaw.

The last glacial period and glacial-interglacial transition were marked by large, millennial-scale climate changes that followed a general north-south pattern, the relative timings of which have been examined for indications of forcing and coupling mechanisms (*1*–*10*). The geographical scale and abruptness of these changes and their apparent absence in the Holocene point to nonlinearities in global climate dynamics and a sensitivity of climate stability to the mean state of the system (*6*, *11*). The stability of a future climate with a mean state forced beyond natural interglacial-Holocene variability is an important issue that is addressable with climate models, but these models first need to be able to reproduce the past behavior before their predictions can be considered robust. Model simulations now can capture some important features of the observed glacial climate changes (*6*), and insights have been gained into the patterns and pacing relationships exhibited in the paleorecords (*12*), but verification depends critically on the ability to synchronize paleorecords and thereby establish the relative timing of millennial-scale changes across the globe.

The observed pattern for the millennial changes in the last glacial period can be summarized as follows. The cold (stadial) phase is interrupted by an abrupt northern warming event (interstadial), then gradual cooling occurs at a rate that may be related to total ice volume (*12*), before a return to glacial conditions. The final return to glacial conditions is frequently marked by a rapid cooling, which is smaller than the initial warming jump. These events, commonly known as Dansgaard-Oeschger (DO) events, are sometimes accompanied by a second series of cooling events, called Heinrich (H) events. H events occur during stadial periods and show little additional cooling signal in Greenland, but are thought to involve much larger changes in thermohaline circulation (*7*). The Antarctic expression of these events is quite

[1]Antarctic Cooperative Research Centre and Australian Antarctic Division, GPO Box 252-80, Hobart, Tasmania, Australia. [2]CNRS/Laboratoire de Glaciologie et Geophysique de l'Environment, 54 Rue Molière, B.P. 96, 38402 St. Martin d'Hères Cedex, France. [3]Institut Pierre-Simon Laplacer Laboratoire des Sciences du Climat et L'Environment, Unite Mixte de Recherche Commissariat à l'Energie Atomique-CNRS 1572, l'Orme des Merisiers, CEA Saclay, 91191 Gif sur Yvette Cedex, France.

*These authors contributed equally to this work.
†Present address: CNRS/Institut de Physique du Globe de Paris, Laboratoire de Cosmochimie et Géochimie, 4 place Jussieu tour 14, 3ème ètage, 75252 Paris Cedex 05, France.
‡To whom correspondence should be addressed. E-mail: tas.van.ommen@utas.edu.au

different: A gradual warming trend precedes DO events by a thousand years or more, with a switch to cooling at around the time of the DO transition from cold to warm conditions. The Antarctic cooling then continues slowly, producing a much more symmetrical waveform than the Greenland temperature record. A clear southern expression is not seen for all DO events, and it has been proposed (*11*) that a major Antarctic event requires a H-DO tandem event as a trigger. The sign and size of the time interval between the southern temperature maximum and the DO transition are a consequence of the coupling mechanism and a valuable constraint on cause and effect. To a lesser extent, there is an association between Greenland cooling jumps and the onset of Antarctic warming that poses a similar constraint where it is sufficiently marked.

Currently, the best synchronization of polar ice-core records in the glacial and transition periods is achieved by matching changes in the composition of the air trapped in bubbles in the ice (*13*). This approach has been used to explore the timing between Antarctic and Greenland temperature records (*1*–*4*, *8*, *10*, *14*, *15*). The observed relationships have been interpreted as consequences of oceanic thermohaline circulation changes (*7*, *16*, *17*) and have led to the concept of a bipolar seesaw (*5*). The seesaw explains antiphase warming and cooling between the poles as the result of large fluctuations in heat transport from the south to the North Atlantic.

In this study, we focus on the deglacial transition from about 17 to 10 thousand years ago (ka). This period was marked by apparently prototypical H-DO changes, namely the Bølling-Allerød (BA) and Younger Dryas (YD) events in the north and the Antarctic Cold Reversal (ACR) in the south. We used the global methane (CH_4) response to these climate events as a marker to establish the sequence of deglacial events at Law Dome (LD), Antarctica. In addition we tied the record to the Greenland Ice Core Project (GRIP) record (*3*) to provide an absolute time scale.

LD is a small (200 km in diameter) ice sheet located at the edge of the Indian Ocean sector of East Antarctica. The core site (*18*), near the summit of LD (66°46′S, 112°48′E), is characterized by a high rate of accumulation (late Holocene average, 0.68 m ice equivalent per year) that results in an ice core with a highly tapered time scale in which the Holocene represents some 93% of the ice thickness of 1200 m. However, the full LD isotopic record generally matches the long records from Vostok and Byrd to at least 80 ka, indicating that the record is continuous and undisturbed over this period. The LD record is suited to gas-synchronization studies because the high accumulation rate and consequent rapid burial give a small age difference (Δage) between trapped air and the older enclosing ice (*13*).

The Glacial-Holocene isotope profiles for LD, Byrd (*19*), European Project for Ice Coring in Antarctica (EPICA), Dome C (EDC) (*9*), and Vostok (*20*) are shown in Fig. 1. The comparative timing of changes depends on the choice of chronology. CH_4 measurements (Fig. 2) are used to tie the LD record to the GRIP time scale (*13*). The Byrd data are likewise presented on a GRIP time scale (*3*). EDC is shown on the EDC1 time scale (*21*), and Vostok on the GT4 time scale (*20*). In the deglacial period, the EDC1 time scale is younger than the GRIP chronology, although the differences are roughly within the EDC1 uncertainty (*21*). In fact, the EDC isotope peak at ~14.2 ka could, from gas ties, be nearly synchronous with the Bølling transition at ~14.5 ka (*9*). The Vostok GT4 time scale is also acknowledged (*20*) as young through the deglacial and beyond the Last Glacial Maximum, particularly when compared to the Sowers (*2*) age scale, derived from matching $\delta^{18}O$ of O_2 to the Greenland Ice Sheet Project 2 core. The slow trapping at Vostok, however, gives relatively large and poorly defined Δage, making the Sowers scale a lower precision chronology (*13*).

We used two chronologies for LD that are based on alternative model assumptions for deriving Δage (*13*). The default chronology gives the larger Δage values (fig. S1D), placing the isotope events earlier in time (Fig. 2). The other chronology (LD_{min}) gives very low Δage values (only ~15 years larger at 15 ka than at present), placing the isotope events as late as can reasonably be supported and providing a limiting scenario.

The ACR marks the period where the Antarctic deglacial warming trend pauses, beginning with a temperature maximum around 14 to 15 ka and ending with resumption of warming 1 to 1.5 thousand years (ky) later. The LD isotope record (Fig. 1) places the ACR earlier than the other records, with onset around 15 ka, up to 1 ky earlier than the Vostok record and ~500 years earlier than the EDC record. Even the LD_{min} chronology places the ACR onset ahead of the Bølling transition at ~14.5 ka (Fig. 2). The noise on the temperature record makes it difficult to pinpoint precisely the time at which the ACR commenced; this is complicated by a small decrease in temperature lasting 1 to 2 centuries that is centered on the broader temperature maximum at the start of the ACR. At this precise depth, the enclosed CH_4 signal is unambiguously pre-Bølling (as illustrated by the markers in Fig. 2). Because the ice must be older than the enclosed gas, this is clearly pre-Bølling ice (*22*).

A similar situation is seen in the timing of the isotopic minimum near 14 ka, which appears earlier in the LD record than in the others. In this case, the methane signal clearly places the minimum somewhere within the Bølling-Allerød (*23*). The occurrence of this minimum close in time to the 14.2-ka meltwater event, MWP1a, and the recent interpretation that this event may have originated in

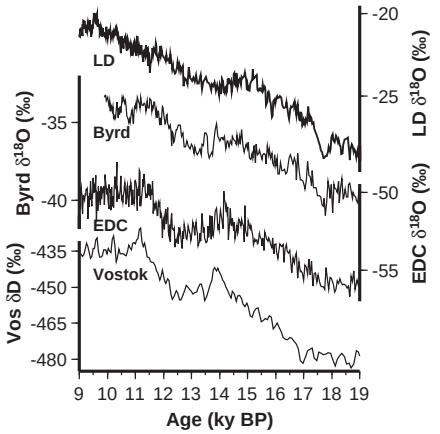

Fig. 1. Deglacial isotope changes for Law Dome (LD) and other Antarctic ice cores from 19 to 9 ky BP, thousand years before the present. The records use various chronologies, as described in the text; time scales for LD and Byrd are both synchronized with GRIP, Greenland, whereas those for EPICA Dome C and Vostok are independently derived. Vos, Vostok; δD, deuterium isotope ratio.

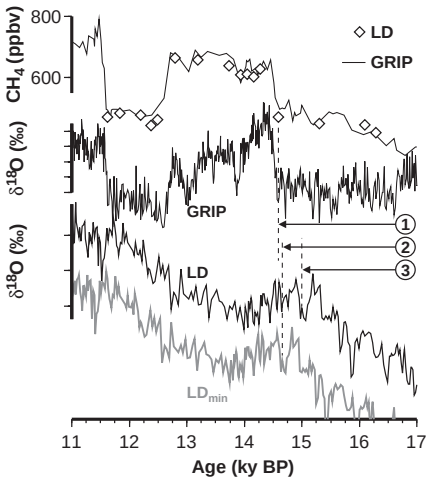

Fig. 2. Expanded view of the Law Dome isotope record under the two scenarios LD_{min} (minimum Δage chronology) and LD (default chronology) with GRIP $\delta^{18}O$ and CH_4 [$\delta^{18}O$ scale unit 1 per mil (‰)]. Marker 1 (M1) indicates the timing of the last pre-Bølling CH_4 measurement. The northern Bølling transition cannot be placed earlier in time than M1. M2 and M3 show the ages of the enclosing ice for the gas sample at M1 under the two Δage scenarios. The intervals M2-M1 and M3-M1 are the Δage values for the LD_{min} and LD scenarios, respectively. Markers M2 and M3 on the isotope curves are located on, or around the peak marking the start of the ACR, which thus cannot be placed later in time than M1 (Δage = 0). ppbv, parts per billion by volume.

Antarctica (*24*) raise the prospect that the two events might be connected.

A consequence of the timings observed here is that the LD ACR is shorter than that at EDC or Vostok. Byrd has similarly been noted (*9*) for its short ACR, but this could be connected to uncertainties in ice flow and dating rather than effects that are climatic in origin. The similarity of the Byrd and LD records from East and West Antarctica tend to support the view that the climatic event was shorter than previously thought. Whether the high East Antarctic Plateau had a different climatic signature is less clear. The relative proximity of LD to the oceanic moisture source during deglacial changes (*25*) could also lead to greater sensitivity and a differing isotopic signature to inland sites.

Another feature of note in the LD record, in the context of north-south asynchrony, is the small cooling jump at about the end of the YD. A close inspection of the record suggests weak antiphase behavior through the YD superimposed on the general warming trend.

Perhaps the largest difference between the LD record and the others is in the period after ~11 ka, during which LD shows prolonged warming before reaching an early Holocene maximum at about 9.5 ka. Timing constraints through this period as determined by $\delta^{18}O$ of O_2 (*13*) do not permit modification to match the early Holocene temperature maxima of Vostok and EDC, which come much earlier, around 11 to 11.5 ka. Even without the O_2 ties, distortion of the time scale to match Vostok and EDC would lead to unreasonable inferred ice-flow or accumulation rate changes. The Byrd record through this period is also considerably different from the East Antarctic records. The difference in the LD record at this time may be connected with the near-coastal core location and the more rapid response of the local ice cap to the deglaciation.

The observations regarding the timing of the ACR relative to North Atlantic changes have implications for models of hemispheric connections and millennial-scale changes. Most consideration has been given to the situation in which North Atlantic thermohaline shutdown, or slowdown, triggers a subsequent warming in the Southern Hemisphere. Precisely how rapidly this change might be propagated is unclear, although modelling (*6*) suggests that the delay would be less than ~100 years. Clearly, this does not accommodate the phasing observed here, with Antarctic cooling or warming occurring before the reverse changes in the north. Our data do not completely rule out essentially synchronous change at the BA transition (to within ~100 years with the LD_{min} chronology), but we emphasize that this is an extreme scenario. Certainly, the second southern trend reversal at the end of the ACR leads the YD onset by ~1 ky.

In most models, control of thermohaline overturning modes is through Northern Hemisphere processes that influence freshwater balance in the North Atlantic; however, one alternative (*26*) proposes control by Antarctic sea ice and associated oceanic salinity changes. In this case, changes in Antarctic temperatures and hydrology, especially for a near-coastal site like LD, could conceivably be detected ahead of the more dramatic shifts that follow thermohaline circulation changes.

Data from both Taylor Dome (*8*) and EDC (*9*) have already been used to show that a bipolar seesaw in temperatures is too simplistic to describe deglacial changes; temperatures decreased simultaneously in the north and south during the Bølling and ACR. The LD results alter the duration of overlap but essentially confirm this observation. The identification of a cause originating in one hemisphere or the other may not be appropriate. A recent examination of the timing statistics for the glacial millennial changes has shown that the south can be equally interpreted as leading or lagging the north (*10*). Further insight may come from alternative interpretations, such as the recently invoked mechanism of "stochastic resonance" (*27*), in which noise in the climate system serves to trigger amplified changes of weak forcing signals; even if the amplifier can be geographically isolated, the noise source(s) essential for crossing thresholds in the system might not.

References and Notes

1. M. Bender *et al*., *Nature* **372**, 663 (1994).
2. T. Sowers, M. Bender, *Science* **269**, 210 (1995).
3. T. Blunier *et al*., *Nature* **394**, 739 (1998).
4. T. Blunier, E. J. Brook, *Science* **291**, 109 (2001).
5. W. S. Broecker, *Paleoceanography* **13**, 119 (1998).
6. A. Ganopolski, S. Rahmstorf, *Nature* **409**, 153 (2001).
7. P. U. Clark, *et al*., *Nature* **415**, 863 (2002).
8. E. J. Steig *et al*., *Science* **282**, 92 (1998).
9. J. Jouzel *et al*., *Geophys. Res. Lett.* **28**, 3199 (2001).
10. E. J. Steig, R. B. Alley, *Ann. Glaciol.*, in press.
11. T. F. Stocker, O. Marchal, *Proc. Natl. Acad. Sci. U.S.A.* **97**, 1362 (2000).
12. M. Schulz, *Geophys. Res. Lett.* **29**, 2-1 (2002).
13. See supporting material on *Science* Online.
14. E. Monnin *et al*., *Science* **291**, 112 (2001).
15. M. Bender, *et al*., *Mechanisms of Millennial Scale Climate Change*, P. Clark, R. Webb, L. Keigwin, Eds. [American Geophysical Union (AGU) Monograph, AGU, Washington, DC, 1999], vol. 112, pp. 149–164.
16. T. F. Stocker, *Quat. Sci. Rev.* **19**, 301 (2000).
17. R. B. Alley, P. U. Clark, *Annu. Rev. Earth Planet. Sci.* **27**, 149 (1999).
18. V. Morgan *et al*., *J. Glaciol.* **43**, 3 (1997).
19. S. J. Johnsen, *et al*., *Nature* **235**, 429 (1972).
20. J.-R. Petit *et al*., *Nature* **399**, 429 (1999).
21. J. Schwander *et al*., *Geophys. Res. Lett.* **28**, 4243 (2001).
22. Exactly how much earlier depends on the adopted Δage and the unconstrained potential for earlier placement of this last gas tie. As an extreme interpretation, recalling that we believe the "young" chronology underestimates Δage, and given the noise on the isotope curve, the ACR commencement may be approximately synchronous with the Bølling transition, but it is difficult to place later.
23. The CH_4 changes in this region do not preclude a younger dating, with the ties in Fig. 2 bunched up toward the YD; however, this leads to anomalous inferred shifts in either ice flow or accumulation through the Bølling-Allerød period that are much less plausible.
24. P. U. Clark *et al*., *Science* **295**, 2438 (2002).
25. B. Stenni *et al*., *Science* **293**, 2074 (2001).
26. R. F. Keeling *et al*., *Paleoceanography* **16**, 112, 330 (2001).
27. A. Ganopolski, S. Rahmstorf, *Phys. Rev. Lett.* **88**, 038501-1 (2002).

28. We acknowledge C. Bourg for $\delta^{18}O$ measurements on trapped air and D. Etheridge for assistance with Δage calculations. V.M. acknowledges travel assistance from LSCE and the Australian Department of Industry, Science, and Technology within the Coordinated French-Australian Collaboration on the Environment.

Supporting Online Material

www.sciencemag.org/cgi/content/full/297/5588/1862/DC1
Materials and Methods
SOM Text
Fig. S1
Tables S1 to S3

22 May 2002; accepted 2 August 2002

Instruction of Translating Ribosome by Nascent Peptide

Feng Gong and Charles Yanofsky*

Expression of the tryptophanase operon of *Escherichia coli* is regulated by catabolite repression and tryptophan-induced transcription antitermination. An induction site activated by L-tryptophan is created in the translating ribosome during synthesis of TnaC, the 24-residue leader peptide. Replacing the *tnaC* stop codon with a tryptophan codon allows tryptophan-charged tryptophan transfer RNA to substitute for tryptophan as inducer. This suggests that the ribosomal A site occupied by the tryptophanyl moiety of the charged transfer RNA is the site of induction. The location of tryptophan-12 of nascent TnaC in the peptide exit tunnel was crucial for induction. These results show that a nascent peptide sequence can influence translation continuation and termination within a translating ribosome.

Recent structural studies with bacterial ribosomes have revealed the features responsible for catalysis of protein synthesis and for antibiotic action. The ribosomal locations of the E, P, and A sites; template RNA; the decoding center; the exit tunnel for the nascent peptide; and the peptidyltransferase center have all been determined (*1–4*). The exit tunnel (*5*), for example, passes through the middle of the 50S subunit and is paved mainly by RNA loops (*1*). Certain nascent peptides when within the peptide exit tunnel can act in cis to alter the